

Sub-microsecond correlations in photoluminescence from InAs quantum dots

Charles Santori,^{*} David Fattal, Jelena Vučković,[†] Glenn S. Solomon,[‡] Edo Waks, and Yoshihisa Yamamoto[§]
*Quantum Entanglement Project, ICORP, JST, E.L. Ginzton Laboratory,
Stanford University, Stanford, California 94305*

(Dated: November 3, 2018)

Photon correlation measurements reveal memory effects in the optical emission of single InAs quantum dots with timescales from 10 to 800 ns. With above-band optical excitation, a long-timescale negative correlation (antibunching) is observed, while with quasi-resonant excitation, a positive correlation (blinking) is observed. A simple model based on long-lived charged states is presented that approximately explains the observed behavior, providing insight into the excitation process. Such memory effects can limit the internal efficiency of light emitters based on single quantum dots, and could also be problematic for proposed quantum-computation schemes.

PACS numbers: 78.67.Hc, 73.21.-b, 42.50.Dv, 78.55.Cr

I. INTRODUCTION

A variety of memory effects have been reported in the optical emission of single semiconductor quantum dots.¹ Many of these effects occur on millisecond timescales, including blinking,^{2,3,4} two-color blinking,⁵ and spectral diffusion.^{6,7} Evidence suggests that millisecond blinking, seen only in a small minority of quantum dots, is caused by nearby defects.⁴ However, we have previously reported a much faster type of blinking that occurs in a majority of quantum dots subject to resonant optical excitation.⁸ This blinking behavior appears as a positive correlation in two-photon coincidence measurements. Blinking has also been observed in diamond color centers,⁹ semiconductor nanocrystals,¹⁰ and in molecules.¹¹ In our case, the correlation timescale depends on the laser excitation power, but can vary from less than 10 ns to at least 800 ns.

This article presents a detailed study of these fast memory effects. In addition to presenting data on the blinking of quantum dots under resonant excitation, we report for the first time negative photon correlations with timescales greater than 100 ns for quantum dots under pulsed excitation with the laser tuned above the bandgap of the host semiconductor. From a physical viewpoint, studying these complimentary memory effects can provide valuable information about the states of a quantum dot, the transitions between them, and especially the nature of the optical excitation process. From a practical viewpoint, blinking effects reduce the efficiency of quantum-optical devices based on single dots,^{8,12,13,14,15,16,17,18} and also bring into question whether quantum dots are stable enough for use in proposed quantum computation schemes that involve optical control.^{19,20} Understanding the mechanisms responsible for these effects is a first step toward being able to suppress them.

Both negative and positive correlations over long timescales can be explained reasonably well through a simplified model presented later in this article. Memory effects imply multiple long-lived configurations of the quantum dot, and our analysis suggests that these are

likely states with differing total charge. As explained below, negative correlations occur because above-band excitation injects electrons and holes into the dot separately, whereas positive correlation (blinking) occurs because resonant excitation injects electrons and holes together, in pairs.

II. SAMPLES

Sample A, the principle sample used in this study, has been described in Refs. 16,18. It contains self-assembled InAs quantum dots (about $25 \mu\text{m}^{-2}$) embedded in the middle of a GaAs spacer layer, and sandwiched between GaAs/AlAs distributed-Bragg-reflector (DBR) mirrors, grown by molecular-beam epitaxy. The quantum dots were grown at a relatively high temperature, which leads to intermixing between the InAs and surrounding GaAs, shortening the emission wavelength to approximately 900-950 nm. Pillars (Fig. 1a) with diameters ranging from $0.3 \mu\text{m}$ to $5 \mu\text{m}$ and heights of $5 \mu\text{m}$ were fabricated in a random distribution by chemically assisted ion beam etching (CAIBE) using sapphire dust particles as etch masks. The resulting microcavities, exhibiting three-dimensional photon confinement,^{21,22} have quality factors of approximately 1000 and spontaneous-emission rate enhancement (Purcell) factors as high as 5. The purpose of the optical microcavity was to enhance the photon collection efficiency and to decrease the spontaneous emission lifetime through the Purcell effect. For this study, the enhanced collection efficiency was valuable, since the data collection rate in photon correlation measurements is proportional to the square of the efficiency.

Sample B, described in Ref. 8, provided additional data for Figs. 5 and 7 below. This sample contained quantum dots (about $11 \mu\text{m}^{-2}$) embedded in simple mesa structures ($0.2\text{-}0.4 \mu\text{m}$ diameter) without optical cavities. The emission wavelengths of these dots were shorter (860-900nm).

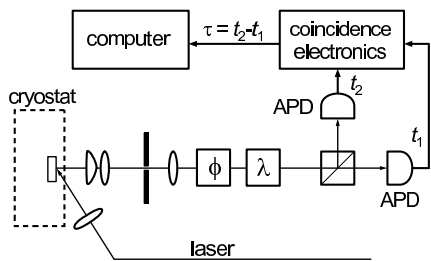


FIG. 1: Schematic diagram of photon correlation setup. ϕ : adjustable half-wave plate followed by a polarizer. λ : spectral filter.

III. EXPERIMENT

The main features of the experimental setups used for acquiring photon correlation data are shown in Fig. 1. This type of setup, known as a Hanbury Brown and Twiss (HBT) setup,²³ has become a common tool for studying the dynamics of single quantum systems, including quantum dots. This measurement technique can be used to characterize the performance of single-photon devices^{8,12,13,14,15,16,17,18} and is more generally useful in studying spectral emission lines and determining how they are connected.^{24,25,26,27,28} For the measurements presented below, several setups were used, but in all cases the samples were held in a cryostat at temperatures ranging from 4-15K and excited from a steep angle (about 54°) by 3 ps pulses every $T_{\text{rep}} = 13$ ns from a mode-locked Ti-Sapphire laser. The emission was collected by a lens (NA=0.5), and imaged onto a pinhole to define a collection region, approximately $6 \mu\text{m}$ wide, on the sample. A single linear polarization was selected by a half-wave plate followed by a fixed polarizer. The emission was then spectrally filtered using a diffraction grating in a monochromator-type configuration, providing spectral resolutions from about 0.1 nm to 0.35 nm for the various setups. The spectral filter allows one to collect just a single emission line of a quantum dot.

The HBT portion of the setup consists of a beamsplitter with each output leading to a photon counter. The photon counters were EG&G SPCM avalanche photodiodes, having about 200 s^{-1} dark counts. The timing resolution varied from about 400 ps to 1.3 ns, depending on how narrowly the light was focused onto the detector active areas. Coincidence electronics, consisting of a time-to-amplitude converter (TAC) followed by a multi-channel analyzer (MCA) computer card, generated a histogram of the relative delay $\tau = t_2 - t_1$ between photon detections at the two counters ($i = 1, 2$) at times t_i .

The two types of memory effects we have observed appear in the photon correlation measurements shown in Fig. 2. The peaks at $\tau = nT_{\text{rep}}$ correspond to events for which one photon was detected from some pulse m , and a second photon was detected from pulse $m+n$. The area of the central peak at $\tau = 0$ gives information about photon number statistics within a single pulse. The side peaks at

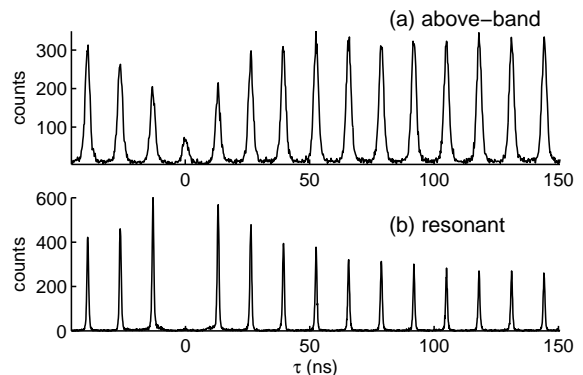


FIG. 2: Photon correlation histograms from quantum dot 1 measured with (a) above-band excitation (750 nm), and (b) resonant excitation (904 nm). The difference in the peak widths between the two cases appears mainly because different setups with different timing resolutions were used.

$\tau \neq 0$ give information on how the emission from different pulses is correlated. Both histograms were obtained from the same quantum dot on sample A, dot 1. The emission was collected from a bright spectral line at about 932 nm, shown in Fig. 3. In Fig. 2(a), the excitation laser was tuned above the bandgap of the GaAs material surrounding the quantum dot, and the excitation intensity was chosen so that the collected emission intensity was far below its maximum value. The decrease of the side peaks near $\tau = 0$ indicates a long-term (27 ns) anti-correlation between photons in consecutive pulses. This is a new effect not previously reported. In Fig. 2(b), the excitation laser was resonant with an excited level of the quantum dot at 904 nm. Such resonances are found through a photoluminescence excitation (PLE) measurement.^{29,30,31} The photoluminescence intensity is monitored as a function of laser wavelength, and typically 2 or 3 peaks are found. The rise of the side peaks in the photon correlation histogram near $\tau = 0$ is opposite from the behavior in (a), and suggests a blinking of the quantum dot between a configuration that can emit light at the wavelength of our spectral filter, and one or more other configurations that cannot emit at this wavelength (but could possibly emit at other wavelengths). The fact that emission from the same quantum dot can have either positive or negative correlations over large timescales, depending on the laser wavelength, implies that there must be an important difference in how carriers are injected into the quantum dot for above-band and resonant excitation.

Fig. 3(a,b) shows photoluminescence spectra from dot 1. The measurements in Fig. 2 were performed on the bright emission line at 932 nm. In (a), the excitation was at 750 nm, above the GaAs bandgap, and many emission lines appear. Some of these are probably from the same quantum dot (trion and biexciton lines, for example) while others could be from other quantum dots. In (b), resonant excitation at 909 nm was used, and most

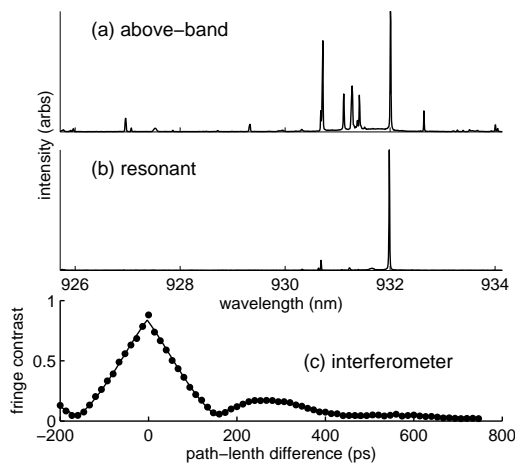


FIG. 3: Spectral data for quantum dot 1: (a) photoluminescence under above-band excitation (750 nm); (b) photoluminescence under resonant excitation (909 nm); (c) measurement from a Michelson interferometer showing fringe contrast vs. path-length difference for the brightest emission line.

of the other peaks have disappeared, demonstrating the selective nature of resonant excitation. Fig. 3(c) shows data obtained by sending light from the main emission line through a Michelson interferometer. This setup is described in Ref. 16 and is similar to the one in Ref. 32. This measurement, performed without a polarizer, reveals fine structure through an oscillation or “beating” in the interference fringe contrast as the path length is varied, indicating that the emission line is actually a doublet with a 13 μeV splitting. Further measurements have shown that the two components have orthogonal linear polarizations, as in Ref. 33. The existence of such a splitting suggests that this line originates from a neutral-exciton transition, rather than a charged-exciton (trion) transition, which would be polarization-degenerate in the absence of a magnetic field.³⁴ For the measurements in Fig. 2, just one component of the doublet was used, selected through polarization.

Several photon correlation measurements taken at different excitation powers are shown in Fig. 4. In this figure, only the normalized areas of the peaks from the measured histograms are shown, plotted versus peak number, with peak 0 at $\tau = 0$. For an ideal $g^{(2)}$ measurement, the normalized peak areas can be written as,

$$g^{(2)}[n] = \frac{\langle n_1[m]n_2[m+n] \rangle}{\langle n_1[m] \rangle \langle n_2[m] \rangle}, \quad (1)$$

where $n_i[m]$ is the number of photons measured on detector i from pulse m . The light source is assumed to be stationary: a shift in m does not change the expectation values in the numerator or denominator. The histogram peak areas obtained from our setup are approximately proportional to the numerator, as long as the mean count rates are small compared with the inverses of the relevant dead times (≈ 50 ns for the photon counters, ≈ 1 μs

for the electronics). The effects of these dead times can also be corrected through calibration relative to scattered laser light. The denominator can be calculated from the mean count rates on the detectors.

For the quantum dots we have studied, when absolute normalization using measured count rates was performed, the peak areas $g^{(2)}[n]$ converged to 1 as $n \rightarrow \infty$, and were well fit by a simple two-sided exponential function:

$$g^{(2)}[n \neq 0] = 1 + g_1 \exp[-(|n| - 1)T_{\text{rep}}/\tau_b], \quad (2)$$

where g_1 and τ_b are fitting parameters that characterize the amplitude and timescale of the memory effect, respectively. This shows that there were no additional blinking effects occurring with timescales greater than τ_b , up to ≈ 100 s. The fits using Eq. 2 typically have errors that can be explained in terms of statistical Poisson \sqrt{N} fluctuations in the measured peak areas. As discussed below, this implies that a two-state Markov process is sufficient to describe the observed memory effects. When absolute normalization was not possible (due insufficient count-rate data), relative normalization was performed by fitting Eq. 2 to the data with an additional fitting parameter, a normalization coefficient multiplied by the entire right-hand side. This procedure was necessary for the data in Fig. 4, while absolute normalization was possible for the data from dots 3, 4, 6, and 7 in Figs. 6 and 7, presented below.

Both the negative and positive correlation effects in Fig. 4 display a strong dependence on laser excitation power. The four measurements in Fig. 4(a) were taken from dot 1 under above-band excitation, while the excitation power was varied to produce mean count rates on one photon counter of 25, 50, 100, and 200 kcps (kilocounts/second), as indicated. The measurements in Fig. 4(b) were taken from dot 2, another quantum dot on sample A (results from this dot appear in Ref. 18). The emission wavelength was 920 nm, and the excitation laser was tuned to a resonance at 905 nm. Four excitation powers were used, 50, 200, 500, and 1200 μW , as indicated. For both data sets, the timescale of the memory effect clearly becomes shorter as the excitation power increases. This suggests that the fluctuations are primarily optically induced, at least for the excitation powers used here.

To enable comparisons between different quantum dots and with theoretical models, the laser excitation powers must be normalized in a useful way. When the excitation intensity is weak, the injection rate of carriers into the dot is expected to be proportional to intensity. However, the efficiency of this process depends on many experimental variables, such as the size of the focused laser spot, the size and shape of the pillar structure containing the dot, and the wavelength of the laser. The collected emission intensity also depends on many factors. In Fig. 5, the emission intensity from three quantum dots under pulsed excitation is plotted as a function of excitation power. In Fig. 5(a), dot 3, another quantum dot on sample A emitting at 919 nm, was excited above-band at 750 nm.

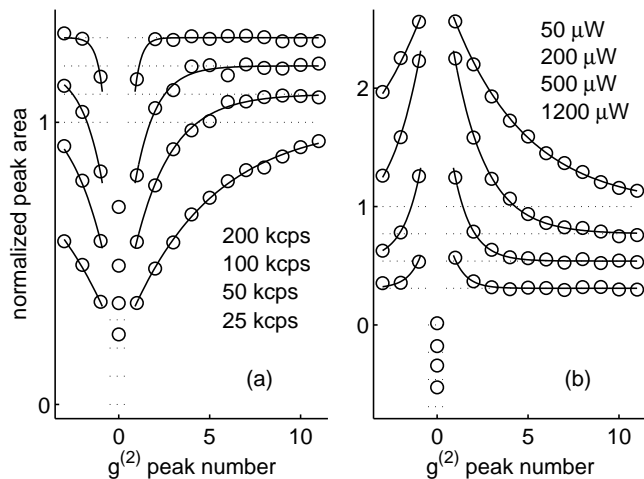


FIG. 4: Normalized peak areas from photon correlation histograms plotted vs. peak number (circles), and two-sided exponential fits (lines) using Eq. 2. (a) Results for dot 1 under above-band excitation, measured at four different excitation powers, resulting in the indicated count rates on one detector. The data sets are shifted vertically for clarity. (b) Results for dot 2 under resonant excitation, measured at four different excitation powers, as indicated.

In Fig. 5(b), dot 2 was excited on resonance at 905 nm. In both cases, a saturation behavior is observed that is well fit by an empirical model,

$$I/I_0 = 1 - e^{-P/P_0}, \quad (3)$$

where I is the measured intensity, P is excitation power, and I_0 and P_0 are constants characterizing the saturation intensity and power, respectively. The normalized excitation power is $p \equiv P/P_0$. This behavior is typical of an “incoherent” excitation process. On the other hand, a simple two-level system without dephasing excited on resonance is expected to undergo Rabi oscillations, characteristic of “coherent” excitation. This behavior can in fact occur in quantum dots when an isolated sharp resonance with little background can be found in the PLE spectrum.^{35,36} Partially coherent behavior is shown in Fig. 5(c) for a quantum dot on sample B emitting at 877 nm and excited at 864 nm. Oscillations in the emission intensity are seen as the laser power is increased. However, the quantum dots discussed elsewhere in this article did not show this coherent effect when excited at the chosen PLE resonances.

Finally, Figs. 6 and 7 summarize the behavior of the memory timescale τ_b and amplitude g_1 , both defined in Eq. 2, as a function of normalized excitation power for several quantum dots. In Fig. 6, dot 3 was excited at 750 nm, above the GaAs bandgap. Fig. 6(a) is a log-log plot showing the fitted value of τ_b/T_{rep} as a function of p . The points approximately follow a line of slope -1 , indicating that the blinking rate $1/\tau_b$ is approximately proportional to the excitation power. The memory timescale can be as long as 130 ns for small excitation powers, and

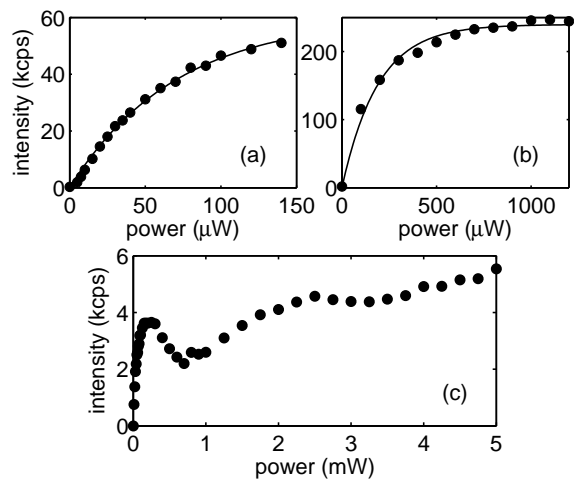


FIG. 5: Mean detector count rate vs. excitation power (circles), plotted for: (a) dot 3 under pulsed above-band excitation; (b) dot 2 under pulsed resonant excitation; (c) a quantum dot on sample B under pulsed resonant excitation, exhibiting coherent excitation behavior. The curves in (a) and (b) are fits using Eq. 3, appropriate for incoherent excitation.

less than one pulse period for large powers. For large enough powers, the memory timescale becomes so short that even the innermost peak areas in the photon correlation histogram have areas close to 1, and it becomes difficult to extract a value for τ_b . Fig. 6(b) is a semilog plot showing the amplitude g_1 as a function of excitation power. Fig. 7 shows similar data for dots 2, 4, 5, 6, and 7 under resonant excitation. Various parameters of these quantum dots are summarized in Table I. Dots 2, 4, 5, and 6 are from sample A, while dot 7 is from sample B. The blinking rate $1/\tau_b$ is again approximately proportional to excitation power below the saturation regime ($P/P_0 < 1$). The memory timescale was as long as 770 ns for dot 4 under weak excitation power. The blinking amplitude g_1 shows similar behavior as with above-band excitation, except that it is positive. The curve fits in these two figures are based on the theoretical model to be introduced next.

IV. THEORETICAL MODEL

The simple exponential decays in the measured photon correlation histograms (Fig. 4, for example) suggest that the memory effects can be described by a two-state Markov process. In such a process, only the most recent state of a system is needed to determine its future evolution. Suppose a quantum dot has two stable states 1 and 2 in which it can remain long after an excitation pulse. The effect of a single excitation pulse is described by:

$$\begin{pmatrix} p_1 \\ p_2 \end{pmatrix} \rightarrow \begin{pmatrix} 1-a & b \\ a & 1-b \end{pmatrix} \begin{pmatrix} p_1 \\ p_2 \end{pmatrix}, \quad (4)$$

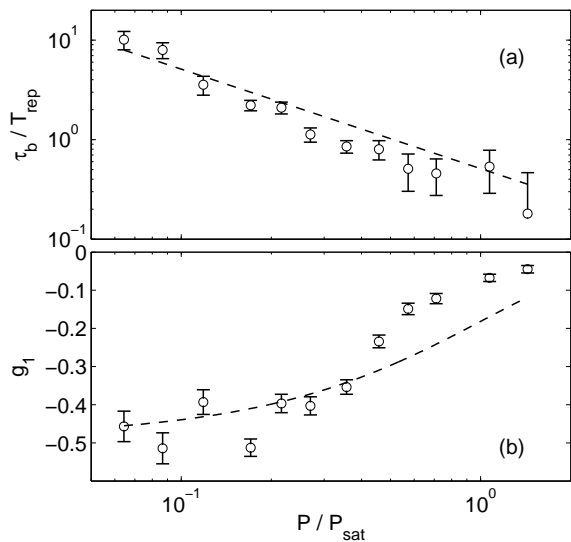


FIG. 6: Summary of results for dot 3 under above-band excitation. Error bars include only Poisson \sqrt{N} fluctuations in the correlation peak areas. (a) Log-log plot showing the fitted blinking timescale τ_b divided by $T_{\text{rep}} = 13$ ns, plotted vs. normalized laser power P/P_0 . The line fit used Eq. 10a with $C_1 = -0.96$. (b) Semilog plot showing blinking amplitude g_1 vs. normalized laser power. The drawn curve used Eq. 10b with $C_2 = 0.51$.

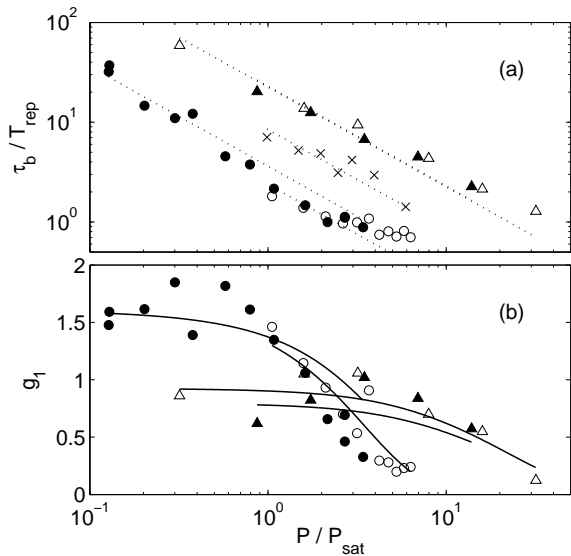


FIG. 7: Summary of results for dots 2 (empty circles), 4 (empty triangles), 5 (filled triangles), 6 (filled circles), and 7 (x's) under resonant excitation. (a) Log-log plot showing the fitted blinking timescale τ_b divided by $T_{\text{rep}} = 13$ ns, plotted vs. normalized laser power P/P_0 . The line fit used Eq. 10a with the C_1 values in Table I. (b) Semilog plot showing blinking amplitude g_1 vs. normalized laser power. The drawn curves used Eq. 10b with the C_2 values in Table I.

where p_i is the probability to be in state i , and a and b are the $1 \rightarrow 2$ and $2 \rightarrow 1$ transition probabilities, respectively. We next assume that, if we have detected a photon immediately after an excitation pulse, the system must have ended in state 1. This is reasonable in our experiment, since we spectrally select an emission line corresponding to a unique transition. If a photon was detected from pulse 0, the system evolves according to,

$$\begin{pmatrix} p_1[m] \\ p_2[m] \end{pmatrix} = \frac{1}{a+b} \begin{pmatrix} b \\ a \end{pmatrix} + \frac{a(1-a-b)^m}{a+b} \begin{pmatrix} 1 \\ -1 \end{pmatrix}, \quad (5)$$

where $p_i[m]$ is the probability of the system to be in state i after pulse m . Finally, let η_i be the probability of emitting a photon immediately after an excitation pulse, given the dot was in state i before the pulse. One can then calculate $g^{(2)}[n]$, obtaining a two-sided exponential function as in Eq. 2 with parameters,

$$\tau_b = \frac{-T_{\text{rep}}}{\ln(1-a-b)}, \quad (6a)$$

$$g_1 = \frac{a(\eta_1 - \eta_2)}{b\eta_1 + a\eta_2}. \quad (6b)$$

If $\eta_1 > \eta_2$, g_1 is positive, as observed experimentally with resonant excitation. If $\eta_1 < \eta_2$, g_1 is negative, as observed with above-band excitation. Another important parameter is the internal efficiency, that is, the probability of emitting a photon after any given excitation pulse. The result is,

$$\eta_{\text{tot}} = \frac{b\eta_1 + a\eta_2}{a+b}. \quad (7)$$

We next consider the nature of states 1 and 2. They can have lifetimes approaching $1\mu\text{s}$, so they cannot be optically active states such as excitons, biexcitons, and trions, which have nanosecond lifetimes. For quantum dot 1 discussed above, spectroscopy suggests that the studied emission line is a neutral-exciton transition, and thus state 1 is the neutral ground state (empty dot). For state 2, the “dark” state, recent spectroscopy literature on self-assembled quantum dots^{34,37,38,39} and chemically synthesized nanocrystals⁴⁰ suggests two main possibilities: a “dark exciton” or a charged state. Dark excitons are electron-hole pairs with spins oriented such that optical recombination is forbidden. Although these states can have microsecond lifetimes in chemically synthesized nanocrystals with typical diameters less than 5 nm, it is unlikely that they could be as long-lived in our self-assembled quantum dots. Self-assembled dots can have reduced symmetry, so that the dark-exciton transition is not entirely forbidden.³⁴ Additionally, if the energy splitting between the bright and dark exciton levels is proportional to the inverse cube of the dot radius,⁴⁰ spin flip processes might occur much faster in our samples, with typical dot radii of 30 nm. Dark excitons in InAs quantum dots have not yet been adequately studied, and

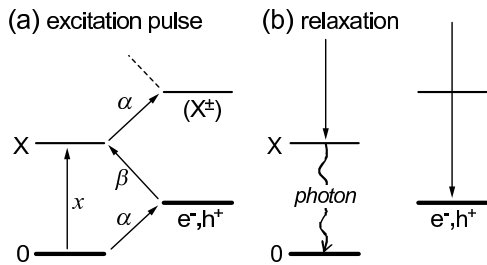


FIG. 8: Energy levels and transitions for the blinking model described in the text: (a) a short period of laser excitation, followed by (b) a long relaxation period.

we cannot reject this possibility with certainty. Nevertheless, we favor the other possibility, that state 2 is a charged state. This choice allows one to explain all of the observed memory effects with a single model. Charge fluctuations in quantum dots under continuous-wave (cw) above-band excitation have been observed through correlations between exciton and trion photon emissions,²⁶ and we have seen similar behavior in our samples. The assumption below is that the extra charges reside inside the quantum dot. An alternative possibility not considered here is that extra charges could be associated with impurities outside the quantum dot; this would not explain the negative correlations observed with above-band excitation.

The model is shown schematically in Fig. 8. Level 0 is the neutral ground state, and level X is the single-exciton state. Level e^-, h^+ is a charged state. There could in reality be more than one charged state involved significantly with the dynamics, but we consider only one charged state in this model. Level X^\pm is a trion (charged-exciton) state. Some of these levels can have degeneracies, but in these cases we are interested only in the total occupation probabilities.

The system evolves in two steps. First, a strong optical field is applied for a short time duration Δt , during which upward transitions are induced. Two of these transitions, with rates α and β , change the total charge of the dot from neutral \rightarrow charged and from charged \rightarrow neutral, respectively. These transitions correspond physically to the capture of single electrons and holes from the surrounding region into the quantum dot. The third transition, with rate x , brings the quantum dot from 0 to X . This transition could occur either through resonant excitation, or through the capture of an entire electron-hole pair. During the second step, which could last several nanoseconds, the system relaxes back down to levels 0 and e^-, h^+ through electron-hole recombination. This is assumed to be a charge-conserving process. If a relaxation occurs from X to 0, a photon is emitted at the special wavelength that our setup detects.

This model can be solved to give the following param-

eters for the general Markov process in Eq. 4:

$$a = \frac{\alpha}{\alpha + \beta}(1 - e^{-(\alpha + \beta)\Delta t}), \quad (8a)$$

$$b = \frac{\beta}{\alpha + \beta}(1 - e^{-(\alpha + \beta)\Delta t}), \quad (8b)$$

$$\eta_1 = 1 - a - e^{-(\alpha + x)\Delta t}, \quad (8c)$$

$$\eta_2 = b. \quad (8d)$$

To fit this model to the experimental data, we make a further assumption, that the rates α , β , and x are proportional to the excitation power p . Inserting Eqs. 8 into Eq. 7 gives the saturation behavior,

$$\eta_{\text{tot}} = \frac{\beta}{\alpha + \beta}(1 - e^{-(\alpha + x)\Delta t}). \quad (9)$$

Comparing this with the empirical Eq. 3 allows the assignment $(\alpha + x)\Delta t = P/P_0 = p$. We then introduce two fitting constants, $C_1 = (x - \beta)/(x + \alpha)$ and $C_2 = \alpha/\beta$. Substituting these and Eqs. 8 into Eqs. 6 gives the final result:

$$\tau_b = \frac{T_{\text{rep}}}{(1 - C_1)p}, \quad (10a)$$

$$g_1 = C_2 \left(\frac{e^{C_1 p} - 1}{e^p - 1} \right). \quad (10b)$$

The parameter C_1 has special significance, since it determines whether electrons and holes are more often added individually or in pairs. If they are added individually ($C_1 < 0$), Eq. 10b predicts negative correlation ($g_1 < 0$) in the detected photons. If they are added more often in pairs ($C_1 > 0$), Eq. 10b predicts positive correlation ($g_1 > 0$). These behaviors have simple qualitative explanations. It follows from Eqs. 1 and 2 that the quantity $1 + g_1$ is proportional to the conditional probability, given that a photon was detected from pulse 0, that a second photon will be detected from pulse 1. When a first photon is detected, the dot is empty immediately afterward. For single-carrier injection, two injections must occur before another photon can be emitted, and thus it is unlikely that another photon will be emitted from pulse 1 if the injection rate is small. The opposite argument applies for the injection of entire electron-hole pairs. If a photon was emitted from pulse 0, it is especially likely that another photon will be emitted from pulse 1, since only a single additional pair needs to be injected. Otherwise, the dot could be charged, in which case the quantum dot will appear dark at the selected wavelength.

The lines in Figs. 6(a) and 7(a) were obtained by fitting Eq. 10a to the measured blinking timescales. The values of C_1 obtained from these fits are summarized in Table I. As expected from the preceding discussion, C_1 is negative for above-band excitation, and positive in all five cases for resonant excitation. Substantial variation in the value of C_1 is seen among the different dots under resonant excitation, however. C_1 is much closer to its maximum

TABLE I: Parameters of the studied quantum dots. λ_0 and λ_{exc} are emission and excitation wavelengths, respectively.

dot #	1	2	3	4	5	6	7*
λ_0 (nm)	932	920	919	938	940	921	876
λ_{exc} (nm)	750/904	905	750	913	904	892	858
P_0 (μ W)	-	190	70	3.1	115	28	446
C_1	-	0.58	-0.96	0.956	0.956	0.72	0.88
C_2	-	2.9	0.51	0.97	0.84	2.2	-

*on Sample B

value of 1 for dots 4 and 5, than for dots 2 and 6. In our model, C_1 characterizes how “clean” the resonant excitation process is, or in other words how rarely extra charges are added and removed from the quantum dot. Perhaps the differences among these dots are related to the emission wavelength. It is also possible that for one or more of these dots, the studied emission line could be a trion (charged exciton) transition. In those cases our model should still apply (after changing the labels in Fig. 8), but it would not be surprising if the values of the fitting parameters were different.

The curves in Figs. 6(b) and 7(b) were obtained by fitting Eq. 10b to the data using the values of C_1 already obtained and using C_2 as a fitting parameter. The fits do not match the data perfectly, a sign that the model is too simple. The saturation regime ($P/P_0 > 1$) is difficult to model accurately, since a large number of states are involved. The model does correctly predict that g_1 tends to zero for large excitation powers, as observed in the data. The parameter C_2 has practical importance, since according to Eq. 9, the maximum internal efficiency at the selected wavelength is $\eta_{\max} = \beta/(\alpha + \beta) = 1/(1 + C_2)$. It should be cautioned, however, that using this formula with the fitted values of C_2 may not give the correct efficiency in the saturation regime, where the model is least accurate.

An important question is why the charge of a quantum dot should ever change when the excitation wavelength is tuned below the GaAs bandgap and below the InAs wetting layer band edge. This could be related to the “wetting layer tail” observed in PLE spectra. This feature has been attributed to continuum states associated with the combined wetting layer-quantum dot system.³⁰ If these states are not localized to a single quantum dot, electrons and holes excited into these states by a laser pulse could be captured by different quantum dots, changing their charges, for example. It has also been suggested that an Auger-type process, which would allow an electron to escape from the quantum dot, could play an important role in the relaxation of electron-hole pairs from excited states.^{41,42} Two-photon processes are an unlikely mech-

anism when the excitation power is far below saturation. This is because the blinking rate $1/\tau_b$ is observed to vary approximately linearly with the excitation power.

V. CONCLUSIONS

We have observed sub-microsecond memory effects in quantum-dot photoluminescence on two samples, one with optical microcavities and one without. Other groups have not yet reported similar behavior, but other studies have not, to our knowledge, explored pulsed resonant excitation, or pulsed above-band excitation far below the saturation level, the two regimes important in our study. These memory effects imply the existence of multiple long-lived states, which are most likely states with different total charge. If this interpretation is correct, it is apparently difficult to prevent the charge of a semiconductor quantum dot from changing during optical excitation.

Fluctuations in the charge of a quantum dot could pose serious difficulties for proposed applications. Light emitters based on single quantum dots will have reduced internal efficiencies at a particular wavelength. Even though the blinking seems to disappear at large excitation powers in photon correlation measurements, our model suggests that the efficiency still suffers, due to the presence of multiple configurations. Optically induced charge fluctuations could also be problematic in schemes for quantum computation that involve optical control of single charges or excitons.

Better stability might be achieved using laser excitation resonant with the fundamental exciton transition. We did not attempt this because of the difficulty of removing scattered laser light, but at least one group has performed single-dot measurements under these conditions.⁴³ Another option might be to design the optical excitation process so that the transition rate into an unwanted configuration is much smaller than the transition rate out of it. In this case, the quantum dot would spend most of its time in the desired configuration. Finally, if charge fluctuations are, in fact, related to continuum states, then fabrication of quantum dots with a low density and without a wetting layer might be advantageous.

Acknowledgments

Supported in part by MURI UCLA/0160-G-BC575. The authors thank A. Scherer and T. Yoshie from Caltech for providing access to CAIBE and for help with fabrication, and M. Pelton for patterning of sample B and for useful comments.

* Electronic address: chars@stanford.edu; Also at Institute of Industrial Science, University of Tokyo, 4-6-1 Komaba,

Meguro-ku, Tokyo 153-8904, Japan

- [†] Department of Electrical Engineering, Stanford University, Stanford, CA 94305
- [‡] Also at Solid-State Photonics Laboratory, Stanford University.
- [§] Also at NTT Basic Research Laboratories, Atsugishi, Kanagawa, Japan.
- ¹ D. Bimberg, M. Grundmann, and N. N. Ledentsov, *Quantum Dot Heterostructures* (John Wiley & Sons, Chichester, 1999).
- ² Al. L. Efros and M. Rosen, Phys. Rev. Lett. **78**, 1110 (1997).
- ³ M-E. Pistol, P. Castrillo, D. Hessman, J. A. Prieto, and L. Samuelson, Phys. Rev. B **59**, 10725 (1999).
- ⁴ M. Sugisaki, H. W. Ren, K. Nishi, and Y. Masumoto, Phys. Rev. Lett. **86**, 4883 (2001).
- ⁵ D. Bertram, M. C. Hanna, and A. J. Nozik, Appl. Phys. Lett. **74**, 2666 (1999).
- ⁶ R. G. Neuhauser, K. T. Shimizu, W. K. Woo, S. A. Empeocles, and M. G. Bawendi, Phys. Rev. Lett. **85**, 3301 (2000).
- ⁷ H. D. Robinson and B. B. Goldberg, Phys. Rev. B **61**, R5086 (2000).
- ⁸ C. Santori, M. Pelton, G. Solomon, Y. Dale, and Y. Yamamoto, Phys. Rev. Lett. **86**, 1502 (2001).
- ⁹ A. Beveratos, S. Kühn, R. Brouri, T. Gacoin, J.-P. Poizat, and P. Grangier, Eur. Phys. J. D, **18**, 191 (2002).
- ¹⁰ M. Kuno, D. P. Fromm, H. F. Hamann, A. Gallagher, and D. J. Nesbitt, J. Chem. Phys. **112**, 3117 (2000).
- ¹¹ S. C. Kitson, P. Jonsson, J. G. Rarity, and P. R. Tapster, Phys. Rev. A **58**, 620 (1998).
- ¹² P. Michler, A. Kiraz, C. Becher, W. V. Schoenfeld, P. M. Petroff, L. Zhang, E. Hu, and A. Imamoglu, Science **290**, 2282 (2000).
- ¹³ V. Zwiller, H. Blom, P. Jonsson, N. Panev, S. Jeppesen, T. Tsegaye, E. Goobar, M-E. Pistol, L. Samuelson, and G. Björk, Appl. Phys. Lett. **78**, 2476 (2001).
- ¹⁴ E. Moreau, I. Robert, J.-M. Gérard, I. Abram, L. Manin, and V. Thierry-Mieg, Appl. Phys. Lett. **79**, 2865 (2001).
- ¹⁵ M. Pelton, C. Santori, J. Vučković, B. Zhang, G. S. Solomon, J. Plant, and Y. Yamamoto, Phys. Rev. Lett. **89**, 233602 (2002).
- ¹⁶ C. Santori, D. Fattal, J. Vučković, G. S. Solomon, and Y. Yamamoto, Nature (London) **419**, 594 (2002).
- ¹⁷ Z. Yuan, B. E. Kardynal, R. M. Stevenson, A. J. Shields, C. J. Lobo, K. Cooper, N. S. Beattie, D. A. Ritchie, and M. Pepper, Science **295**, 102 (2002).
- ¹⁸ J. Vučković, D. Fattal, C. Santori, G. S. Solomon, and Y. Yamamoto, Appl. Phys. Lett. **82**, 3596 (2003).
- ¹⁹ A. Imamoglu, D. D. Awschalom, G. Burkard, D. P. DiVincenzo, D. Loss, M. Sherwin, and A. Small, Phys. Rev. Lett. **83**, 4204 (1999).
- ²⁰ Filippo Troiani, Ulrich Hohenester, and Elisa Molinari, Phys. Rev. B **62**, R2263 (2000).
- ²¹ J. M. Gérard, B. Sermage, B. Gayral, B. Legrand, E. Costard, and V. Thierry-Mieg, Phys. Rev. Lett. **81**, 1110 (1998).
- ²² G. S. Solomon, M. Pelton, and Y. Yamamoto, Phys. Rev. Lett. **86**, 3903 (2001).
- ²³ F. T. Arecchi, M. Corti, V. Degiorgio, and S. Donati, Opt. Commun. **3**, 284 (1971).
- ²⁴ E. Moreau, I. Robert, L. Manin, V. Thierry-Mieg, J. M. Gérard, and I. Abram, Phys. Rev. Lett. **87**, 183601-1 (2001).
- ²⁵ D. V. Regelman, U. Mizrahi, D. Gershoni, E. Ehrenfreund, W. V. Schoenfeld, and P. M. Petroff, Phys. Rev. Lett. **87**, 257401-1 (2001).
- ²⁶ A. Kiraz, S. Fälth, C. Becher, B. Gayral, W. V. Schoenfeld, P. M. Petroff, L. Zhang, E. Hu, and A. Imamoglu, Phys. Rev. B **65**, 161303-1 (2002).
- ²⁷ C. Santori, D. Fattal, M. Pelton, G. S. Solomon, and Y. Yamamoto, Phys. Rev. B **66**, 045308 (2002).
- ²⁸ R. M. Stevenson, R. M. Thompson, A. J. Shields, I. Farrer, B. E. Kardynal, D. A. Ritchie, and M. Pepper, Phys. Rev. B **66**, 081302 (2002).
- ²⁹ H. Kamada, H. Ando, J. Temmyo, and T. Tamamura, Phys. Rev. B **58**, 16243 (1998).
- ³⁰ Y. Toda, O. Moriwaki, M. Nishioka, and Y. Arakawa, Phys. Rev. Lett. **82**, 4114 (1999).
- ³¹ J. J. Finley, A. Lemaitre, A. D. Ashmore, D. J. Mowbray, M. S. Skolnick, M. Hopkinson, and T. F. Krauss, Phys. Stat. Sol. (b) **224**, 373 (2001).
- ³² C. Kammerer, G. Cassabois, C. Voisin, M. Perrin, C. Delalande, Ph. Roussignol, and J. M. Gérard, Appl. Phys. Lett. **81**, 2737 (2002).
- ³³ V. D. Kulakovskii, G. Bacher, R. Weigand, T. Kümmell, A. Forchel, E. Borovitskaya, K. Leonardi, and D. Hommel, Phys. Rev. Lett. **82**, 1780 (1999).
- ³⁴ M. Bayer, G. Ortner, O. Stern, A. Kuther, A. A. Gorbunov, A. Forchel, P. Hawrylak, S. Fafard, K. Hinzer, T. L. Reinecke, S. N. Walck, J. P. Reithmaier, F. Klopff, and F. Schäfer, Phys. Rev. B **65**, 195315-1 (2002).
- ³⁵ H. Kamada, H. Gotoh, J. Temmyo, T. Takagahara, and H. Ando, Phys. Rev. Lett. **87**, 246401-1 (2001).
- ³⁶ H. Htoon, T. Takagahara, D. Kulik, O. Baklenov, A. L. Holmes, and C. K. Shih, Phys. Rev. Lett. **88**, 087401 (2002).
- ³⁷ M. Bayer, O. Stern, A. Kuther, and A. Forchel, Phys. Rev. B **61**, 7273 (2000).
- ³⁸ A. Hartmann, Y. Ducommun, E. Kapon, U. Hohenester, and E. Molinari, Phys. Rev. Lett. **84**, 5648 (2000).
- ³⁹ J. J. Finley, P. W. Fry, A. D. Ashmore, A. Lemaitre, A. I. Tartakovskii, R. Oulton, D. J. Mowbray, M. S. Skolnick, M. Hopkinson, P. D. Buckle, P. A. Maksym, Phys. Rev. B **63**, 161305-1 (2001).
- ⁴⁰ Al. L. Efros, M. Rosen, M. Kuno, M. Nirmal, D. J. Norris, and M. Bawendi, Phys. Rev. B **54**, 4843 (1996).
- ⁴¹ J. Urayama, T. B. Norris, J. Singh, and P. Bhattacharya, Phys. Rev. Lett. **86**, 4930 (2001).
- ⁴² S. Sanguinetti, K. Watanabe, T. Tateno, W. Wakaki, N. Koguchi, T. Kuroda, F. Minami, and M. Gurioli, Appl. Phys. Lett. **81**, 613 (2002).
- ⁴³ N. H. Bonadeo, Gang Chen, D. Gammon, and D. G. Steel, Phys. Stat. Sol. (b) **221**, 5 (2000).